Origin and Migration of the Alpine Iceman
Wolfgang Müller, *et al.*
Science **302**, 862 (2003);
DOI: 10.1126/science.1089837

onic carbonate lysocline and helped prevent extreme Paleozoic glaciation.

One prediction of our hypothesis is that a relationship should exist between the thickness of post-glacial cap carbonate facies and excess alkalinity accumulated in the ocean during glaciation. We calculate that within 50 thousand years (ky) of sea level rise, 2.8×10^{18} to 7.1×10^{18} mole equivalents (mol eq) of accumulated alkalinity, equivalent to 1.4×10^{18} to 3.5×10^{18} mol $CaCO_3$, was lost through precipitation, with more than 50% of the loss occurring in less than 10 ky (Fig. 3C). This is sufficient to form a carbonate layer that averages between 0.8 and 2.1 m thick and assumes a shelf area three times that of the present day (modern shelfal area being some 2.0×10^7 km^2). This agrees well with typical cap (dolostone) thicknesses observed in shelfal settings of order meters (*5*, *7*, *23*). Thus, the occurrence of post-glacial cap carbonates is quantitatively consistent with a coral reef–like mechanism, with rapid deposition on newly flooded continental shelves taking place from a highly oversaturated ocean (*6*). Methane hydrate degradation (*7*) need only then add a portion of the required alkalinity.

The established framework for understanding Neoproterozoic glaciation envisages the onset of a completely frozen world through catastrophic ice-albedo feedback—the "snowball Earth" hypothesis (*4*, *5*). An alternative climatic interpretation is of ice-free equatorial waters coexisting with low-latitude ice sheets (*24*–*26*). Although this has the advantage of providing a substantive refugium for multicellular life (*2*, *26*), it has been rejected because of the need to account for the inferred longevity of glaciation and the occurrence of cap carbonates (*5*, *27*). Our geochemical hypothesis answers both these deficiencies and predicts relatively stable atmospheric CO_2 consistent with the radiative forcing required by the open-water climate solution (*25*) (Fig. 3A).

The evolution of calcareous organisms marking the beginning of the Phanerozoic and the subsequent development of a responsive deep-sea carbonate sink drove a fundamental increase in the stability of the Earth's carbon-climate system, limiting the extremity of glaciation possible. Before this, the weakly stabilizing neritic carbonate sink would have been the Achilles' heel of the Precambrian climate system.

References and Notes

1. L. E. Sohl, N. Christie-Blick, D. V. Kent, *Geol. Soc. Am. Bull.* **111**, 1120 (1999).
2. B. Runnegar, *Nature* **405**, 403 (2000).
3. J. C. Crowell, *Pre-Mesozoic Ice Ages: Their Bearing on Understanding the Climate System*, *Geol. Soc. Am. Mem.* **192** (1999).
4. P. F. Hoffman, A. J. Kaufman, G. P. Halverson, D. P. Schrag, *Science* **281**, 1342 (1998).
5. P. F. Hoffman, D. P. Schrag, *Terra Nova* **14**, 129 (2002).
6. M. J. Kennedy, *J. Sediment. Res.* **66**, 1050 (1996).
7. M. J. Kennedy, N. Christie-Blick, L. E. Sohl, *Geology* **29**, 443 (2001).
8. K. Caldeira, M. R. Rampino, *Paleoceanography* **8**, 515 (1993).
9. J. D. Milliman, *Global Biogeochem. Cycles* **7**, 927 (1993).
10. W. H. Berger, *Naturwissenschaften* **69**, 87 (1982).
11. G. Munhoven, L. M. François, *J. Geophys. Res.* **101**, 21423 (1996).
12. A. J. Ridgwell, A. J. Watson, M. A. Maslin, J. O. Kaplan, *Paleoceanography*, doi:10.1029/2003PA000893, in press.
13. J. C. G. Walker, B. C. Opdyke, *Paleoceanography* **10**, 415 (1995).
14. S. K. Boss, B. H. Wilkinson, *J. Geol.* **99**, 497 (1991).
15. We used the PANDORA ocean carbon cycle model (*28*) coupled to a representation of the preservation and burial of $CaCO_3$ in deep-sea sediments (*29*) in a model configuration essentially the same as that used elsewhere (*8*, *11*, *13*). We provided long-term negative feedback by modifying weathering fluxes (*13*) of carbon (15 Tmol year^{-1}) and alkalinity (40 Tmol year^{-1}) according to the (pre–vascular plant) formulation of GEOCARB (*21*), while leaving volcanic CO_2 outgassing (5 Tmol year^{-1}) (*13*) constant. We made no additional reduction in global weathering rates because of glaciation, consistent with recent analysis of the late Quaternary glacial geochemical system (*30*). The presence or absence of planktic calcifiers was simulated by setting the surface ocean export ratio of $CaCO_3$ to organic matter in PANDORA to 0.2 or 0.0, respectively. We assumed the surface ocean was initially in equilibrium with atmospheric CO_2 at 3400 ppmv [sufficient to prevent the formation of ice sheets in climate models of the Neoproterozoic (*24*)] and with Ω at 6.5 with respect to aragonite (except where otherwise noted in Table 1), consistent with a Neoproterozoic ocean more highly saturated than at present (*18*, *23*). Carbon and alkalinity inventories (Fig. 3, B and C) were thus uniquely determined (assuming present-day [Ca^{2+}]). The value of the $CaCO_3$ precipitation rate scaling constant, k, was set to achieve initial steady state (Table 1). Although variability in the carbonate carbon isotopic ratio is a distinctive feature of the Neoproterozoic geological record (*4*, *5*, *7*), without explicit representation of the controls on organic carbon burial, its interpretation cannot be advanced here.
16. S. J. Zhong, A. Mucci, *Geochim. Cosmochim. Acta* **57**, 1409 (1993).
17. N. Leclercq, J. P. Gattuso, J. Jaubert, *Global Change Biol.* **6**, 329 (2000).
18. R. Riding, *Sedimentology* **47**, 179 (2000).
19. V. Ramaswamy *et al.*, in *Climate Change 2001: The Scientific Basis*, J. T. Houghton *et al.*, Eds. (Contribution of Working Group I to the Third Assessment Report of the Intergovernmental Panel on Climate Change, Cambridge Univ. Press, New York, 2001), pp. 349–416.
20. K. Caldeira, *Geology* **19**, 204 (1991).
21. R. A. Berner, *Science* **249**, 1382 (1990).
22. R. A. Wood, J. P. Grotzinger, J. A. D. Dickson, *Science* **296**, 2383 (2002).
23. J. P. Grotzinger, A. H. Knoll, *Palaios* **10**, 578 (1995).
24. T. J. Crowley, W. T. Hyde, W. R. Peltier, *Geophys. Res. Lett.* **28**, 283 (2001).
25. S. K. Baum, T. J. Crowley, *Geophys. Res. Lett.* **28**, 583 (2001).
26. W. T. Hyde, T. J. Crowley, S. K. Baum, W. R. Peltier, *Nature* **405**, 425 (2000).
27. D. P. Schrag, P. F. Hoffman, *Nature* **409**, 306 (2001).
28. W. S. Broecker, T.-H. Peng, *Radiocarbon* **28**, 309 (1986).
29. A. J. Ridgwell, A. J. Watson, D. E. Archer, *Global Biogeochem. Cycles* **16**, 1071, doi:10.1029/2002GB001877 (2002).
30. I. W. Jones, G. Munhoven, M. Tranter, P. Huybrechts, M. J. Sharp, *Global Planet. Change* **33**, 139 (2002).

31. Supported by NSF and the Trusthouse Charitable Foundation (A.J.R.).

23 June 2003; accepted 26 September 2003

Origin and Migration of the Alpine Iceman

Wolfgang Müller,[1]* Henry Fricke,[2] Alex N. Halliday,[3] Malcolm T. McCulloch,[1] Jo-Anne Wartho[4]

The Alpine Iceman provides a unique window into the Neolithic-Copper Age of Europe. We compared the radiogenic (strontium and lead) and stable (oxygen and carbon) isotope composition of the Iceman's teeth and bones, as well as $^{40}Ar/^{39}Ar$ mica ages from his intestine, to local geology and hydrology, and we inferred his habitat and range from childhood to adult life. The Iceman's origin can be restricted to a few valleys within ~60 kilometers south(east) of the discovery site. His migration during adulthood is indicated by contrasting isotopic compositions of enamel, bones, and intestinal content. This demonstrates that the Alpine valleys of central Europe were permanently inhabited during the terminal Neolithic.

A well-preserved human mummy, the "Iceman," was recovered from a glacier located at the main Alpine watershed between Italy and Austria in 1991. The Iceman was ~46 years old and lived ~5200 years ago. Both the mummy and its associated equipment provided unprecedented insights into daily life during the late Neolithic-Copper Age of central Europe (*1*–*4*). One of the remaining questions regarding the Iceman is his place of origin. Molecular genetic analyses suggest that the Iceman's mitochondrial DNA closely resembles that of central and northern Europeans, including people from the Alpine region (*5*). Poor preservation prevented the recovery of nuclear DNA, thereby restricting better spatial resolution of his origin (*5*, *6*). For the Iceman's late adulthood, his southern origin in present-day northern Italy has been deduced from the pollen and moss contents of his intestine (*7*, *8*). The lack of pottery among his

[1]Research School of Earth Sciences, The Australian National University, Canberra, ACT 0200, Australia. [2]Department of Geology, Colorado College, 14 East Cache La Poudre Street, Colorado Springs, CO 80903, USA. [3]Department of Earth Sciences, ETH Zürich, CH-8092 Zürich, Switzerland. [4]Department of Applied Geology, Curtin University of Technology, GPO Box U1987, Perth, WA 6845, Australia.

*To whom correspondence should be addressed. E-mail: wolfgang.mueller@anu.edu.au

equipment prevented a conclusive archaeological analysis regarding his affinity to northern or southern cultures (*2*, *9*), although a southern origin has been favored (*3*, *10*).

We completed a comprehensive radiogenic (Sr and Pb) and stable (O and C) isotope study of samples of the Iceman representing different ontogenetic stages to determine his birthplace, habitat, and range (*11*). These samples include tooth enamel, dentine, cortical and trabecular bone, intestinal content, and his clothing and equipment. Enamel and bone represent archives of childhood and adulthood, respectively (*12*), whereas his activities during his last days can be inferred from the intestinal content. Isotopic tracing is based on the transfer (via nutrition) of the isotopic signatures of soils and waters into biominerals (*13*). Radiogenic isotopes allow provenance determination relative to the local geological environment, because different lithologies show systematic isotopic variations caused by the decay of long-lived radionuclides. Within the Iceman's potential habitat, at least four lithological units can be distinguished isotopically, including Mesozoic limestones, Permian volcanics (rhyolite), Eocene basalts, and a heterogeneous group of phyllites and polymetamorphic gneisses (Fig. 1). Stable isotopes provide information about altitude, latitude, or position relative to a watershed (oxygen) or paleodiet (carbon) (*14*, *15*). The oxygen isotopic composition ($\delta^{18}O$) of precipitation can be reconstructed from $\delta^{18}O$ in human biogenic apatite after correction for metabolically induced isotopic fractionation (*16*), because oxygen in biominerals is predominately derived from ingested water. Spatial variations in $\delta^{18}O$ of precipitation arise from the preferential rainout of $H_2{}^{18}O$ from air masses during overland transport, making precipitation at higher altitudes or further inland systematically depleted in ^{18}O. This is crucial for constraining the Iceman's origin, because he was found at an Alpine watershed, where there is considerable altitude contrast (Fig. 1). Areas north of the watershed predominately capture precipitation from the cooler Atlantic Ocean with long transport distances, whereas the nearby warmer Mediterranean Sea supplies water masses to the south. As a result, $\delta^{18}O$ values of precipitation in the north are expected to be lower than those south of the watershed (*17*, *18*).

This is confirmed by the oxygen isotopic ratios presented here, which for rivers north of the Alpine watershed (in Austria) are ~1 to 2 per mil (‰) lower than for southern rivers (in Italy) at similar longitude [for example, the Ötz versus the Schnals valley (Figs. 1 and 2A and table S1 (*11*)]. Areas near low-altitude passes such as the southern Wipp and Langtaufers valleys are influenced by both moisture sources because there is a limited amount of transfer across the watershed. Superimposed on the north-to-south variation is an overall lowering of riverine $\delta^{18}O$ toward the west of the study area. Contributions of precipitation from the highest altitudes (that is, snow melt) make river water more negative in $\delta^{18}O$ than small streams and springs, which at inhabited terraces above forested valleys are the likelier source of drinking water (Fig. 2A). Overall, the least-depleted $\delta^{18}O$ values are found in the southeast of the area, in the Eisack/Isarco, Rienz, Hohlen, and Non valleys. Convert-

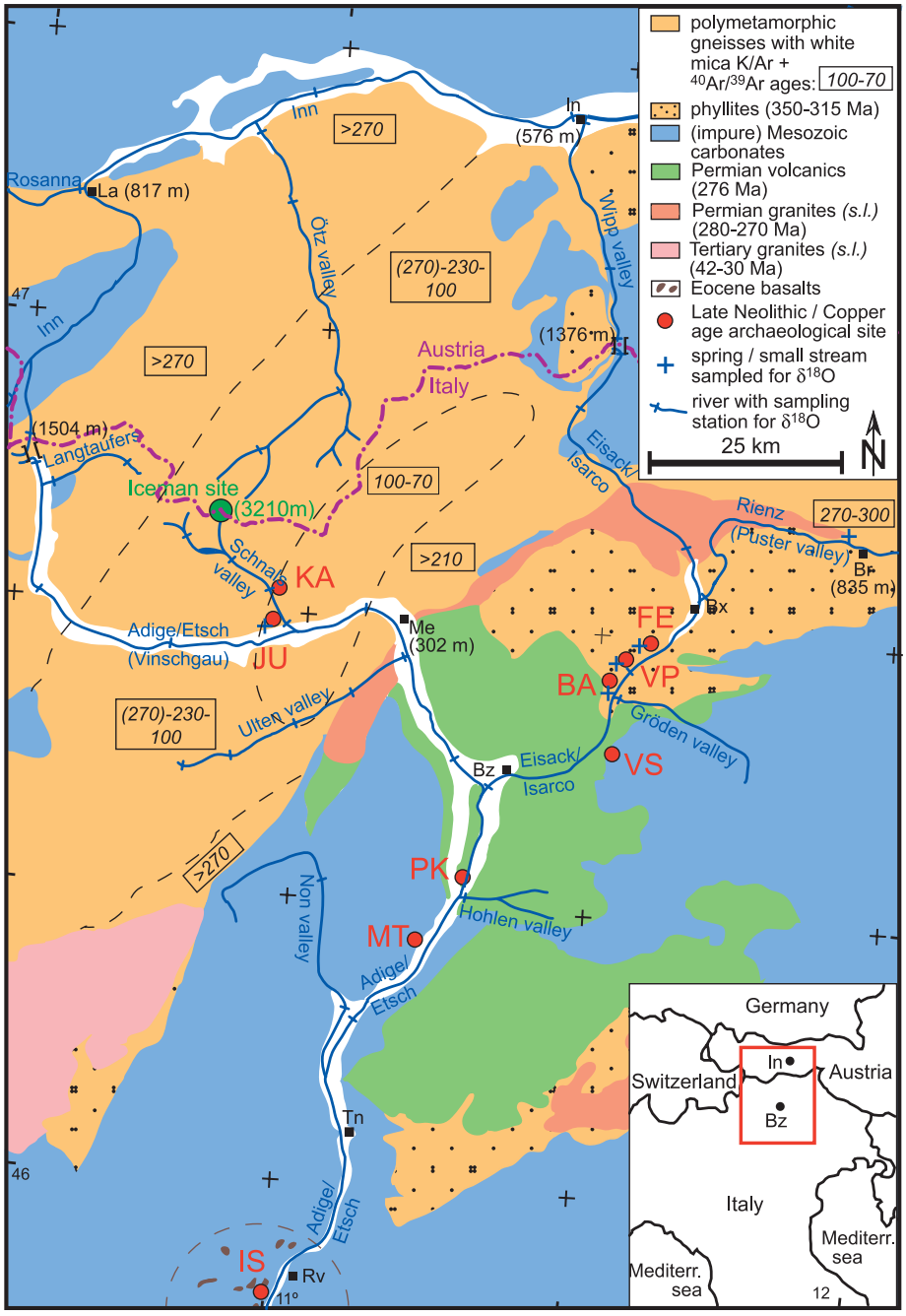

Fig. 1. Simplified geological-lithological map of the study area, showing the main lithologies that can be distinguished using radiogenic isotopes (supporting online text). The decrease in white mica ages (ages are shown in boxes) in polymetamorphic gneisses from northwest to southeast reflects the increasing overprint of an older (Variscan: ~330 Ma) by a younger (Alpine: ~90 Ma) metamorphic event (*26*). Values in parentheses indicate altitude in meters. The Alpine watershed runs along the border between Austria and Italy. Abbreviations are as follows. Archaeological sites: BA, Barbian; FE, Feldthurns; IS, Isera; JU, Juval; KA, Katharinaberg; MT, Margreid-Tolerait; PK, Pigloner Kopf; VP, Villanders/Plunacker; VS, Völs. Present-day towns: Br, Bruneck/Brunico; Bx, Brixen/Bressanone; Bz, Bozen/Bolzano; In, Innsbruck; La, Landeck; Me, Meran/Merano; Rv, Rovereto; Tn, Trento.

ing (*16*) the $\delta^{18}O$ values of the Iceman's enamel to equivalent water values, it is inferred that he was drinking water with $\delta^{18}O$ values between –10.6‰ (first premolar) and –11.0‰ (canine) when he was 3 to 5 years of age (table S1). These values are important because only waters south of the Alpine watershed have such high values (Fig. 2A). Cortical and trabecular bone samples indicate that during adulthood, the Iceman was drinking water with $\delta^{18}O$ values of –11.7 and –11.4‰, respectively. These $\delta^{18}O$ bone values are considered reliable because ice from the Iceman site yielded lower $\delta^{18}O$ values (–13.4 to –16.4; the range may reflect varying contributions of northern and southern moisture sources). Postmortem alteration by meltwater would shift trabecular bone more toward lower $\delta^{18}O$ values, yet the opposite is observed. Additionally, we converted $\delta^{18}O$ data from present-day human enamel taken from third molars to equivalent water values (table S1) and found that they reproduced the observed $\delta^{18}O$ values of corresponding streams and springs (Fig. 2A and supporting online text). Different valleys (such as the Eisack versus the Etsch/Adige) show resolvable clusters of $\delta^{18}O$ teeth values, with the single outlier for each valley being explained by unaccounted-for migration. The interpretation of the Iceman's $\delta^{18}O$ record assumes that relative differences in $\delta^{18}O$ observed for present-day waters also existed ~5200 years ago, which is corroborated by a speleothem from a cave located ~110 km SE of the Iceman site. It records only minor fluctuations [~0.3‰ $\delta^{18}O_{PDB}$; as measured relative to the Pee Dee belemnite (PDB) standard] and similar $\delta^{18}O$ values between 5350 to 5100 years ago and today (*19*).

Radiogenic isotope analysis was used to refine how far south the Iceman lived (table S2). Soil leachates (*11*) of the four main lithologies have distinct Pb-Sr isotopic compositions, although some overlap exists for the Permian volcanics and the gneiss/phyllite groups (Fig. 2B). These data are the basis for comparison with the radiogenic isotopic compositions of the Iceman's samples (*11*). Enamel fragments from all three teeth are characterized by uniformly high $^{87}Sr/^{86}Sr$ ratios of 0.7203 to 0.7206 for the main dissolution step (Fig. 2B and fig. S1). The smaller canine enamel fragment (3sm, Fig. 2C) records a higher Sr isotopic ratio of 0.7215, whereas for adjacent dentine, this value is only marginally higher than for the other three enamels. This allows the relative timing of all tooth fragments to be established, because enamel mineralizes a few months earlier than adjacent dentine (*20*), making the small canine piece the earliest formed tooth fragment. Its higher Sr isotopic signature may indicate a different diet during earliest childhood. Two cortical femur bone samples have lower $^{87}Sr/^{86}Sr$ ratios of 0.7175 and 0.7181, whereas for trabecular bone, this value is 0.7184 [final dissolution steps (Fig. 2B and fig. S1)]. In contrast to enamel, all bone leachates yield higher Sr isoto-

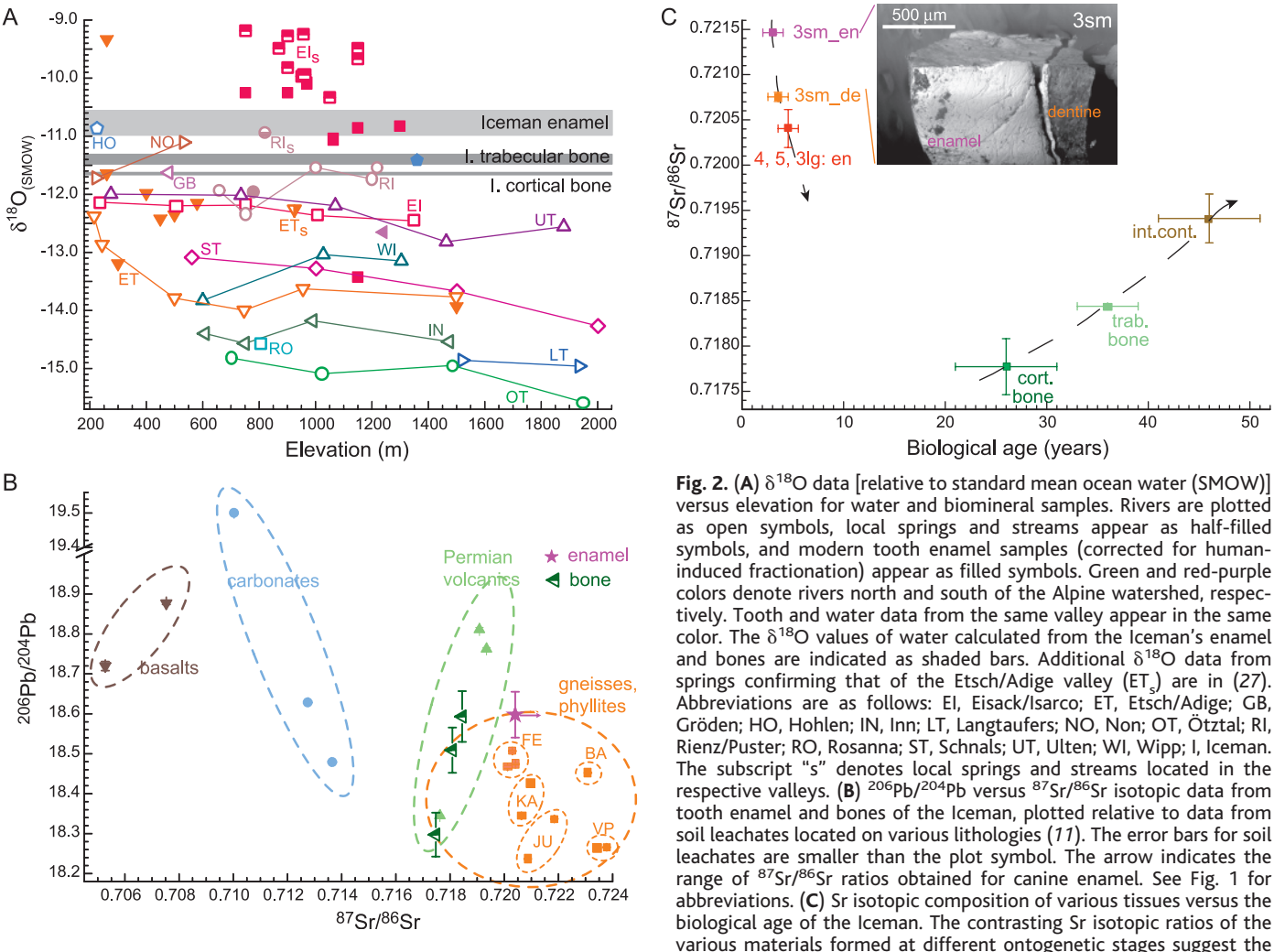

Fig. 2. (**A**) $\delta^{18}O$ data [relative to standard mean ocean water (SMOW)] versus elevation for water and biomineral samples. Rivers are plotted as open symbols, local springs and streams appear as half-filled symbols, and modern tooth enamel samples (corrected for human-induced fractionation) appear as filled symbols. Green and red-purple colors denote rivers north and south of the Alpine watershed, respectively. Tooth and water data from the same valley appear in the same color. The $\delta^{18}O$ values of water calculated from the Iceman's enamel and bones are indicated as shaded bars. Additional $\delta^{18}O$ data from springs confirming that of the Etsch/Adige valley (ET_s) are in (*27*). Abbreviations are as follows: EI, Eisack/Isarco; ET, Etsch/Adige; GB, Gröden; HO, Hohlen; IN, Inn; LT, Langtaufers; NO, Non; OT, Ötztal; RI, Rienz/Puster; RO, Rosanna; ST, Schnals; UT, Ulten; WI, Wipp; I, Iceman. The subscript "s" denotes local springs and streams located in the respective valleys. (**B**) $^{206}Pb/^{204}Pb$ versus $^{87}Sr/^{86}Sr$ isotopic data from tooth enamel and bones of the Iceman, plotted relative to data from soil leachates located on various lithologies (*11*). The error bars for soil leachates are smaller than the plot symbol. The arrow indicates the range of $^{87}Sr/^{86}Sr$ ratios obtained for canine enamel. See Fig. 1 for abbreviations. (**C**) Sr isotopic composition of various tissues versus the biological age of the Iceman. The contrasting Sr isotopic ratios of the various materials formed at different ontogenetic stages suggest the Iceman's migration during life (indicated by dashed lines). The inset shows a scanning electron photomicrograph of the smaller composite canine fragment. Data on the mineralization of enamel, dentine, and bones are from (*15*, *20*), whereas the Iceman's biological age is from (*4*). Abbreviations are as follows: 3, canine; 4, first premolar; 5, second premolar; sm, small; lg, large; en, enamel; de, dentine; cort., cortical; trab., trabecular; int. cont., intestinal content.

pic ratios than the final dissolution. This is interpreted to reflect incipient postmortem alteration of bones due to interaction with high $^{87}Sr/^{86}Sr$ meltwater, which is consistent with ice cores closest to the Iceman that have high $^{87}Sr/^{86}Sr$ ratios of 0.723 to 0.729 (supporting online text). Immersion of the Iceman's body in water has also been deduced from the skin composition, trace elements in bones, and the distribution of artefacts (*21*–*23*). Lower $^{87}Sr/^{86}Sr$ ratios for the enamel leachates do not record water-related alteration but are consistent with limited passive exchange of the outermost enamel with saliva having $^{87}Sr/^{86}Sr < 0.720$ during adulthood, as deduced from the Iceman's bones. Dentine, having been shielded by enamel, has a uniform Sr isotopic composition. Enamel and bone Sr isotopic compositions of the final dissolution steps have to be regarded as close, but nevertheless minimum and maximum values for childhood and adulthood, respectively.

A comparison of Sr-Pb isotopic compositions of the Iceman's enamel with various soils reveals that regions dominated by limestones, basalts, and Permian volcanics can be excluded as being the Iceman's childhood area (Fig. 2B). These regions include the lower Etsch valley south of Bolzano and further south (Fig. 1). Instead, the enamel Sr-Pb isotopic signature is consistent with compositions of gneisses and phyllites, which occur near the Iceman site or in Schnals valley, Vintschgau [the Etsch/Adige valley (N)W of Merano], Ulten valley, middle Eisack valley, and lower Puster valley (Fig. 1). These interpretations based on Sr-Pb isotopes are consistent with $\delta^{18}O$ data, because precipitation south of the lower Etsch/Adige valley (*18*) has higher $\delta^{18}O$ values than inferred from the Iceman's biominerals. Similarly, regions far north of the Iceman site (north of Inn valley) that may record $\delta^{18}O$ signatures of precipitation (*17*) compatible with the Iceman can be excluded on the basis of the prevalence of limestones (Fig. 1). The Sr-Pb isotopic composition of the Iceman's bones apparently matches those of Permian volcanics; however, it is known that other gneiss/phyllite areas are characterized by lower Sr isotope values, which overlap with the Permian volcanics (*24*, *25*).

A sample of the Iceman's intestinal content was screened for cereal fragments (*8*) in order to constrain the origin of his last meal. Because not enough fragments were present, the entire sample was analyzed for its Sr isotopic composition, which is intermediate between the enamel and cortical bone compositions and continues the trend already indicated by trabecular bone (Fig. 2C). This intestinal sample also contained 12 100- to 400-μm white micas that are believed to have been ingested as a result of the grinding of cereal or from drinking water (supporting online text). These micas were individually analyzed for their $^{40}Ar/^{39}Ar$ ages (table S3), which is important because Permian volcanics, phyllites, and polymetamorphic gneisses exhibit different geological ages as a result of their different magmatic/metamorphic evolution during the Alpine [~90 million years ago (Ma)] and Variscan (~330 Ma) orogenies (*26*) (Fig. 1). The resultant white mica ages range between 95 and 300 Ma (with one at 440 Ma), with one broad peak between 160 and 220 Ma (seven micas) and a narrower peak between 285 and 300 Ma (three micas; fig. S2). This age distribution is found in the gneiss lithology only and excludes the Permian volcanics (276 Ma) and the phyllites (315 to 350 Ma). It demonstrates that the Iceman lived on gneissic soils during his later adulthood. Moreover, the variable but elevated Sr isotopic ratios of the Iceman's clothing and equipment (table S2) indicate that the Iceman used both animal and plant materials from a wider area located on gneiss/phyllite soils.

Our data indicate that the Iceman spent his entire life in the area south of the discovery site, which is consistent with palaeobotanical (*7*, *8*) and most archaeological analyses (*2*, *3*, *10*) but extends earlier investigations into his childhood. This contrasts with a previous study (*24*) that concluded that the Iceman lived his final years in the Ötztal area north of the Alpine watershed. This was based on a comparison of trace elemental ratios and $\delta^{18}O$ values between the Iceman's bones and soil-buried medieval bones (supporting online text).

Archaeological sites located on terraces in the Eisack valley record the closest match in $\delta^{18}O$ values between the Iceman's enamel and modern human enamel (Figs. 1 and 2A). Furthermore, one site, Feldthurns, reveals the closest match in Sr-Pb isotopes between the Iceman's enamel and local soils (Fig. 2B). Excavations in Feldthurns have produced a menhir typical of the Copper Age of the region (*3*); thus, this may have been the region of the Iceman's childhood. Because areas with incompatible isotopic signatures can be excluded with greater certainty than positive assignments can be made, other potential childhood areas include the lower Puster valley (river Rienz), the lowest Vinschgau (Etsch valley) near Merano, and the Ulten valley. However, no archaeological sites from that period are known from the Ulten valley. Conversely, the different isotopic composition of the Iceman's bones argues for a different food source and hence migration to a region with distinct soil and water composition during his adulthood (Fig. 2C). This is also indicated by differences in $\delta^{13}C$ between enamel and bone (table S1). More negative $\delta^{18}O$ values in bone indicate migration to slightly higher altitudes or further to the northwest, where $\delta^{18}O$ in precipitation is lower. Besides Sr-Pb-O isotopes, the white mica $^{40}Ar/^{39}Ar$ age distribution from his intestine, especially the 95-Ma age, is consistent only with a small area ~10 to 20 km SW-NW of Merano in lower Vinschgau (the Etsch valley). Among others, this includes the site of Juval, which has been favored as the home of the Iceman during his adulthood (*23*). However, Juval has a Sr-Pb isotopic composition incompatible with that of the Iceman's bones (Fig. 2B).

An alternative scenario to that of permanent resettlement is seasonal migration, such as the Iceman's involvement in transhumance between low-altitude settlements in the south and summer grazing areas above the timberline in the north (such as southern Ötztal), which started in the Middle Neolithic and is still practiced today (*23*). If the $\delta^{18}O$ value of ~ –11‰ is taken to represent lower elevations, then the $\delta^{18}O$ data of –11.7 and –11.4‰ for his cortical and trabecular bones are consistent with a decreasing residence during adult life (from ~2 months to ~1 month per year, respectively) in the southern elevated parts of Ötztal, with $\delta^{18}O$ values of water of ~ –15‰. An indication of the validity of this scenario may be the $^{87}Sr/^{86}Sr$ ratio of the Iceman's intestinal wall (table S2), which is similar to that of his earliest enamel and could represent the integrated value of his final few weeks or months during the late winter–early spring period.

References and Notes

1. H. Seidler *et al.*, *Science* **258**, 455 (1992).
2. R. Prinoth-Fornwagner, T. R. Niklaus, *Nucl. Instrum. Methods Phys. Res. B* **92**, 282 (1994).
3. A. Fleckinger, H. Steiner, *The Fascination of the Neolithic Age—The Iceman* (Folio, Bolzano, Italy, 1999).
4. O. Gaber, in *Die Gletschermumie aus der Kupferzeit—Neue Forschungsergebnisse zum Mann aus dem Eis* (Folio, Bolzano, Italy, 1999), vol. 1, pp. 39–44.
5. O. Handt *et al.*, *Science* **264**, 1775 (1994).
6. M. G. Thomas *et al.*, paper presented at The Iceman 2001, Bozen/Bolzano, Italy, 20 to 22 September 2001.
7. J. H. Dickson, S. Bortenschlager, K. Oeggl, R. Porley, A. McMullen, *Proc. R. Soc. London Ser. B* **263** (1996).
8. K. Oeggl, in *The Iceman and his Natural Environment*, S. Bortenschlager, K. Oeggl, Eds. (Springer, Vienna, 2000), vol. 4, pp. 89–116.
9. J. Winiger, *Br. Archaeol. Rep. Int. Ser.* **701**, 246 (1998).
10. K. Spindler, *The Man in the Ice: The Preserved Body of a Neolithic Man Reveals the Secrets of the Stone Age* (Weidenfeld and Nicolson, London, 1994).
11. Materials and methods are available as supporting material on *Science* Online.
12. P. Budd, J. Montgomery, J. Evans, C. Chenery, in *Plasma Source Mass Spectrometry: The New Millennium*, J. G. Holland, S. D. Tanner, Eds. (Royal Society of Chemistry Special Publication, Cambridge, 2001), vol. 267, pp. 311–326.
13. A. Sillen, G. Hall, S. Richardson, R. Armstrong, *Geochim. Cosmochim. Acta* **62**, 2463 (1998).
14. K. Rozanski, L. Araguas-Araguas, R. Gonfiantini, in *Cli-*

mate Change in Continental Isotopic Records, P. K. Swart, Ed. (American Geophysical Union, Washington, DC, 1993), vol. 78, pp. 1–36.
15. F. D. Pate, *J. Archaeol. Method Theory* **1**, 161 (1994).
16. A. Longinelli, *Geochim. Cosmochim. Acta* **48**, 385 (1984).
17. G. Humer, D. Rank, P. Trimborn, W. Stichler, *Niederschlagsisotopenmessnetz Österreich* (Umweltbundesamt, Vienna, Austria, 1995), vol. 52.
18. A. Longinelli, E. Selmo, *J. Hydrol.* **270**, 75 (2003).
19. F. McDermott *et al.*, *Quat. Sci. Rev.* **18**, 1021 (1999).
20. H. J. M. van Waes, P. W. Stöckli, *Kinderzahnmedizin, Farbatlanten der Zahnmedizin* (Thieme, Stuttgart, 2001), vol. 17.
21. T. L. Bereuter, W. Mikenda, C. Reiter, *Chem. Eur. J.* **3**, 1032 (1997).
22. C. Kralik, W. Kiesl, H. Seidler, W. Platzer, W. Rabl, in *Human Mummies*, K. Spindler, H. Wilfling, E. Rastbichler-Zissernig, D. zur Nedden, H. Nothdurfter, Eds. (Springer, Vienna, 1996), vol. 3, pp. 283–287.
23. K. Oeggl, J. H. Dickson, S. Bortenschlager, in *The Iceman and His Natural Environment*, S. Bortenschlager, K. Oeggl, Eds. (Springer, Vienna, 2000), vol. 4, pp. 163–166.
24. J. Hoogewerff *et al.*, *J. Archaeol. Sci.* **28**, 983 (2001).
25. P. Horn, personal communication.
26. M. Thöni, *Schweiz. Mineral. Petrogr. Mitt.* **79**, 209 (1999).
27. C. Spötl, M. Unterwurzacher, A. Mangini, F. J. Longstaffe, *J. Sediment. Res.* **72**, 793 (2002).
28. We thank the South Tyrol Museum of Archaeology, Bozen/Bolzano (Autonome Provinz Bozen, Italy), especially E. Egarter Vigl and A. Fleckinger, for access to samples, which made this study possible. We are grateful to G. Bonani, S. Bortenschlager, L. Dal Ri, C. Marzoli, K. Oeggl, A. Pedrotti, K. Spindler, and P. Tropper for supplying samples or help during sampling. K. Alt, S. Eggins, S. Frisia, E. Hammerle, P. Horn, W. Kutschera, M. Meier, G. Mortimer, K. Oeggl, A. Pedrotti, W. Rigott, M. Shelley, H. Spiss, C. Spötl, S. Stowe, U. Tecchiati, and two anonymous reviewers are thanked for discussions and help. This research was supported by the Australian Research Council, Colorado College, ETH Zürich, and the Swiss National Science Foundation.

Supporting Online Material
www.sciencemag.org/cgi/content/full/302/5646/862/DC1
Materials and Methods
SOM Text
Figs. S1 and S2
Tables S1 to S3
References

30 July 2003; accepted 29 September 2003

Cyclic Dynamics in a Simple Vertebrate Predator-Prey Community

Olivier Gilg,[1,2]* Ilkka Hanski,[1] Benoît Sittler[3]

The collared lemming in the high-Arctic tundra in Greenland is preyed upon by four species of predators that show marked differences in the numbers of lemmings each consumes and in the dependence of their dynamics on lemming density. A predator-prey model based on the field-estimated predator responses robustly predicts 4-year periodicity in lemming dynamics, in agreement with long-term empirical data. There is no indication in the field that food or space limits lemming population growth, nor is there need in the model to consider those factors. The cyclic dynamics are driven by a 1-year delay in the numerical response of the stoat and stabilized by strongly density-dependent predation by the arctic fox, the snowy owl, and the long-tailed skua.

The cyclic dynamics of boreal and arctic populations of small rodents is one of the most intensively studied phenomena in population ecology. Many (*1*–*4*), although not all (*5*, *6*), researchers now agree that the most likely mechanism that maintains cyclic dynamics in boreal vole populations is predation by specialist mustelid predators. In contrast, interaction with food resources is thought to drive the dynamics of at least some lemming populations (*7*). Even in the case of vole dynamics, competition among prey for space or food is thought to play a key role in halting prey population growth at high density, thereby allowing the predator population to catch up with their faster-reproducing prey (*1*, *3*, *8*–*10*).

One of the simplest vertebrate predator-prey communities is that of lemmings and their dependent predators in the high-Arctic tundra in Greenland. It constitutes only one mammalian prey, the collared lemming (*Dicrostonyx groenlandicus*), and four predators, the stoat (*Mustela erminea*), the arctic fox (*Alopex lagopus*), the snowy owl (*Nyctea scandiaca*), and the long-tailed skua (*Stercorarius longicaudus*) (*11*, *12*). The open tundra landscape and the continuous daylight in summer in the high Arctic provide particularly favorable conditions for fieldwork on vertebrate predators. We studied the densities, breeding success, and diet of the four predators in a 75-km^2 area in the Karup Valley in northeast Greenland (72°30′ N, 24°00′ W), from 1988 to 2002.

Lemming densities were estimated with live trapping for 1998 to 2002 (*11*, *13*) and with regression between live-trapping results and lemming winter nest counts (*12*, *14*) for the other years (*15*). The winter nests of lemmings are made of grass within snow beds and are easily located on the ground after snowmelt. We made a complete count of the nest numbers in an area of 15 km^2 every spring for 1988 to 2002. Although a varying number of lemmings may use the same nest (*16*, *17*), the winter nest count in our large study area should closely reflect the actual number of lemmings. The correlation between the spring densities, as estimated by live trapping, and the winter nest count for the years 1998 to 2002 is high ($R^2 = 0.99$, $P < 0.01$) (fig. S1).

The stoat density was estimated from the number of lemming winter nests predated and occupied by stoats in the 15-km^2 area (*12*, *13*). Stoats always use lemming nests in winter, and stoat-occupied nests are easily distinguished by the abundance of lemming fur within the nest (*12*, *18*).

Daily predation rates were plotted against the current (daily) lemming density (N) to estimate functional responses of predators. Daily predation rates were estimated from scat samples for arctic foxes ($n = 927$) and stoats ($n = 663$), from direct observations for skuas (n=475 hours), and from pellet samples and direct observations for snowy owls ($n = 3419$ pellets and 245 hours of observation). In the open landscape and in the continuous daylight of summer, the behavior of individual predators can be closely monitored over areas as large as 5 km^2.

Predator densities were plotted against lemming density at snowmelt to estimate numerical responses. With the exception of the stoat, separate responses were estimated for adults and weaned or fledged young (*15*).

The daily consumption rate of the avian predators is somewhat higher than that of the mammalian predators, but the latter are more efficient at catching prey at low lemming densities (predation half-saturation constant < 0.2 lemmings/ha) than are the former (≥ 1) (Fig. 1, upper row). The numerical responses of the predators are species specific. The nomadic snowy owl only settles and breeds in areas where lemming density at snowmelt (N') exceeds a threshold of $\approx$2 lemmings/ha. The constant adult density in summer of the migratory long-tailed skua is five times as high as that of the snowy owl when the latter is present, but the skua breeds successfully only when $N' > 1$. The arctic fox shows elevated breeding success when $N' > 1$ but maintains a relatively constant adult density, except in peak lemming years ($N' \approx 10$) (Fig. 1, middle row), when fox density may increase greatly.

The stoat is the only predator that shows a delayed response to changes in prey density, with highest numbers seen the year after the lemming peak (Fig. 2, top). The results for the

[1]Department of Ecology and Systematics, Division of Population Biology, Post Office Box 65, 00014 University of Helsinki, Finland. [2]CBGP, Campus de Baillarguet, Equipe Biologie et Gestion des Pullulations (INRA-IRD), CS 30016, 34988 Montferrier/Lez Cedex, France. [3]Institut für Landespflege, University of Freiburg, 79085 Freiburg, Germany.

*To whom correspondence should be addressed. E-mail: olivier.gilg@libertysurf.fr